Received: 4 April 2022 | Accepted: 30 October 2022

DOI: 10.1002/ls.1632

RESEARCH ARTICLE

WILEY

Tribology of dust-stop seals of mixing machines

Ehsan Fatourehchi[1] | **Hamed Shahmohamadi**[1] | **Ramin Rahmani**[1] | **Homer Rahnejat**[1,2] | **Mark Johnson**[3] | **Ian Wilson**[3]

[1]Wolfson School of Mechanical, Electrical and Manufacturing Engineering, Loughborough University, Leicestershire, UK

[2]School of Engineering, University of Central Lancashire, Preston, UK

[3]Farrel Ltd, Rochdale, UK

Correspondence
Ramin Rahmani, Wolfson School of Mechanical, Electrical and Manufacturing Engineering, Loughborough University, Leicestershire, UK.
Email: r.rahmani@lboro.ac.uk

Funding information
Innovate UK

Abstract

Dust stop seals are widely used in powder and rubber mixing industries. Design of the sealing system requires a continuous supply of pressurised lubricant, which is not recycled because of the risk of contamination. There is also the potential of large volume leakage of oil due to poor sealing, increasing operational costs and necessitating remedial measures to avoid environmental protection. Furthermore, the seal faces are prone to failure in relatively short periods of time due to reduced gap and lubricant leakage. The paper presents an analytical method and numerical predictions based on Reynolds equation under combined hydrodynamic and hydrostatic conditions with the entrant lubricant through hydraulically loaded feedholes. The validity of these methods is ascertained through comparison with a more complex but time-consuming solution of Navier–Stokes equations. The numerical predictions allow for determining the prevailing tribological contact conditions and assessing its suitability for evaluating the sealing performance of mixing machinery.

KEYWORDS

computational fluid dynamics, dust-stop seals, friction, hydrodynamics, hydrostatics, load carrying capacity, oil leakage

1 | INTRODUCTION

Mechanical face seals are critical components of many machines. They are used extensively as contacting or non-contacting lubricated devices[1,2] or as gas seals in pipeline systems.[3,4] Their variety and differing operating conditions give rise to a broad range of conjunctional behaviour from hydrostatics to hydrodynamics, as well as their combined effects with incompressible, compressible or turbulent flow conditions.[5–7] The current study deals with dust-stop seals of industrial internal batch mixer chambers. These mixers are used to process rubber compounds. The seals should be effective in order to prevent the escape of mixture from the chamber. To achieve this requirement, a pair of ring seals is mounted onto the mixer shaft. The design of the dust-stop seals is primarily based upon hydrostatic mechanism of lubrication, where the pressurised oil from a hydraulic pumping system is injected into the seal contact through feed-holes. The lubricated seal faces are usually loaded through springs and/or a hydraulic pressurising system. Nevertheless, the leakage of the mixed compound from the chamber onto the sealing conjunction occurs,

Abbreviations: 2D, two-dimensional; 3D, three-dimensional; CFD, computational fluid dynamics; FDM, finite difference method; FVM, finite volume method; PEEK, polyether ether ketone; PSOR, point successive over-relaxation method.

often causing abrasive wear of seal faces, as well as adverse environmental issues. Additionally, loss of sealing often leads to significant leakage of lubricant which aside from exacerbating environmental pollution also adds to the operational cost of mixing machines. Furthermore, any ingression of the lubricating oil into the mixing chamber can compromise the quality of the mixture and thus the final intended product.

The use of lubricant-free dust-stop seals has been suggested in order to avoid the aforementioned problems associated with oil leakage. Such solutions seek to utilise thermoset materials such as cured carbon fibre reinforced polyimide and fibre reinforced polyetheretherketone (PEEK) thermoplastics.[8] However, such solutions require further reinforcement and strengthening of the polymer matrix to counter the effect of abrasive particles, amongst other issues. In the meantime, it seems that a combination of research for enhancing the seal ring surface material properties and making provisions to improve the design of lubrication system would enhance the performance of the next generation of mixing machinery.

As noted by Key et al.,[9] the principal means of generating pressure in flat-face seals is through hydrostatic load carrying capacity, where the gap between the seal faces must converge from high-pressure side to lower pressures in the radial direction for a stable sealing performance. However, this is not always possible for a multitude of reasons, such as the use of low viscosity fluid (to counter viscous friction) or low sealing pressures at high operating temperatures. In such cases, shallow or deep slots or recesses called hydropads are added to one of the seal faces. In the case of shallow hydropads, the maximum generated pressure is achieved when the depth of hydropad is of the order of lubricant film thickness.[9] Interestingly, the similar finding is reported for optimum performance of textured surfaces.[10,11] In fact, the arrangement of oil feedholes in the contact of dust-stop seals is analogous to the hydrostatic pocket seals. The specific design of such pockets and their in-flow patterns have been studied extensively, for example by Braun and Dzodzo,[12] who investigated the effect of pocket shape on the flow pattern and generated pressure distribution in pocket seals using 2D Navier–Stokes equations. They showed various swirl patterns inside the pockets with different geometries. They concluded that the fluid inertial effects may appear downstream of pocket's exit irrespective of that generated through shear or the jet flow strength. Shen et al.[13] also reported the results of a combined experimental–CFD numerical study on the effect of pocket geometry on the performance of thrust pad hydrostatic bearings for machine tool applications.

The current study strives to establish an analytical-numerical approach to study the tribology of dust-stop seals. The developed analytical model is based on the principle of operation of hydrostatic seals. However, due to the specific design of the sealing face, including the oil feedholes, it is anticipated that an analytical hydrostatic approach, despite of its simplicity and convenience, particularly for application as a design tool for industry, would not provide sufficiently accurate description of the in-situ conditions. For instance, the hydrostatic model does not provide any information about the extent of the lubricated area occurring between the positions of consecutive oil feedholes. Furthermore, it is not possible to take into account the waviness of surfaces caused during the process of manufacture. Therefore, a numerical model based on the solution of Reynolds equation is developed to take into account both hydrostatic and hydrodynamic effects. A primary aim of the study is to develop models to enhance the understanding of prevailing conditions and guide the development of a suitable test-rig. The predictions of analytical and numerical models are compared with those from a more detailed CFD analysis, which includes the effect of fluid inertia for lubricant leakage through relatively large emerging gaps. This problem can occur due to poor sealing performance. Such a comprehensive analysis of dust-stop seals has not hitherto been reported in the literature.

2 | SEALING ARRANGEMENT

The mixing machines investigated here are utilised to mix rubber compounds in the presence of additional mixing elements, providing final compounds with desired physical and chemical properties, intended for various applications. Figure 1a shows an internal rubber batch mixer as an example of such machinery. A pair of seals in this configuration is shown in Figure 1b. These are mounted upon the rotating mixing shaft at its exit from the chamber. The split gland ring constitutes the stationary part, and the wear ring is the rotating face of the contact.

3 | THEORETICAL ANALYSIS

Three different predictive methods are developed and used in the current study. These are

i. an analytical approach, based on the principle of hydrostatic bearing analysis.
ii. a combined hydrostatic and hydrodynamic numerical approach, based on the solution of 2D Reynolds equation.
iii. a CFD approach, providing a 3D detailed flow analysis in the sealing conjunction.

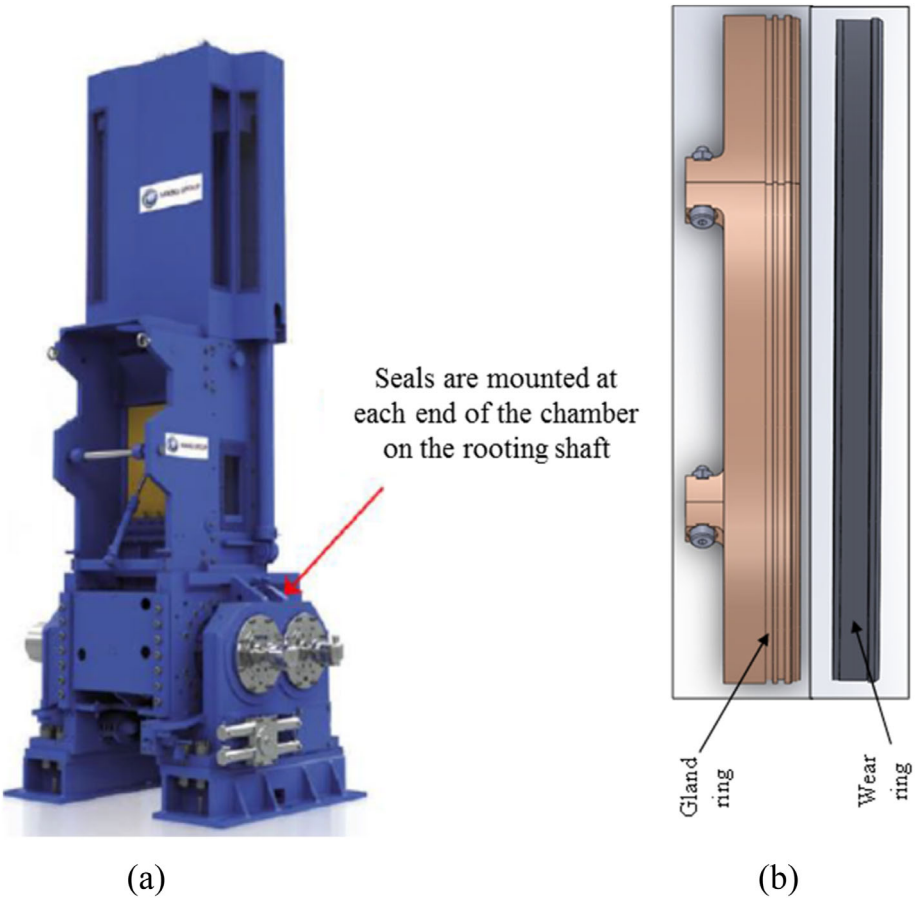

FIGURE 1 (a) Internal rubber batch mixer and (b) schematic configuration of a sealing ring pair

The aim of the analytical model is to provide a quick and industrially efficient analysis tool. However, it lacks the inclusion of finer details. Furthermore, its suitability for modelling existing dust stopper seals has not yet been ascertained. On the other hand, the 2D model based on numerical solution of the Reynolds equation is expected to provide finer predictions of the prevailing conditions, including any variations in the surface features away from the oil feedholes, but with the drawback of additional modelling complexity and time-intensive computations. The aim of the CFD analysis is to provide further fine-tuning and establish a good understanding of the underlying physics of fluid flow. It is a useful tool to investigate the importance of some aspects such as inertial fluid flow but can only be limited to the analysis of a segment of the seal because of computational costs. CFD is also used for the purpose of validation of the other two models.

3.1 | Analytical hydrostatic lubrication model

An analytical model is developed, based on the hydrostatic bearing concept. Owing to geometrical symmetry with peripheral placement of oil feedholes, a single oil feed-hole can be isolated for the purpose of analysis as shown in Figure 2. As the seal contact is exposed to the ambient pressure at its inner and outer rims, it is assumed that the higher pressure region of the contact around an oil feedhole would expand into a circular region of a radius $r_o - r_i$. A further simplification is to convert the elliptical shape of the recess cross-section around the oil feedhole into an equivalent circular cross-section with an equivalent area. Therefore, an equivalent radius of $r_0 = \sqrt{ab}/2$ can be considered for this circular cross-section.

Assuming purely Poiseuille radial flow from an oil feedhole to the edges of the equivalent circular recess, the mass flow rate at each oil feed-hole may be obtained as[14]:

$$\dot{m} = \frac{\pi \rho_r p_r h_0^3}{6\eta_r} \left[\frac{1}{\ln\left(\frac{r_o - r_i}{2r_0}\right)} \right]. \quad (1)$$

The generated load carrying capacity at the considered portion of the seal contact, including the inner recess area is obtained as[14]:

$$W_c = \frac{3\eta_r \dot{m}}{\rho_r h_0^3} \left[\left(\frac{r_o - r_i}{2}\right)^2 - r_0^2 \right]. \quad (2)$$

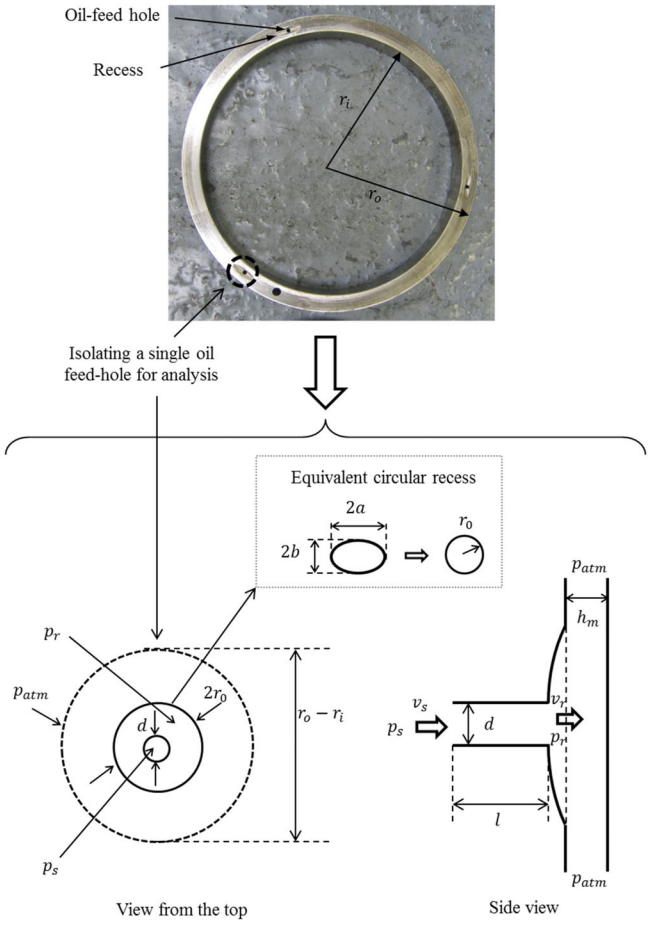

FIGURE 2 Modelling a single pressurised oil feed-hole contact

To take into account, the pressure drop in the oil supply line, and assuming that the opposing seal face would act as a baffle, the Bernoulli's principle can be used between the lubrication pump and the exit from the recess. For a single oil feed-hole line, neglecting any change due to the gravitational head, this can be expressed as follows:

$$\frac{p_s}{\rho_s}+\frac{v_s^2}{2}=\frac{p_r}{\rho_r}+\frac{v_r^2}{2}+f_l\frac{l}{d}\frac{v_s^2}{2}+K\frac{v_s^2}{2}, \tag{3}$$

where the last two terms on the right-hand side of Equation (3) account for the losses through Darcy–Weisbach relationship.[15] The loss coefficient for a laminar flow ($\mathrm{Re}_d < 2320$), which is the case in the current study, is given as: $f_l = 64/\mathrm{Re}_d$. However, for a gradual enlargement such as in the case of a recess with an opposing surface proximate to the oil feed line exit, the minor loss coefficient becomes a function of the angle of expansion and the ratio of the inlet and outlet diameters, as well as the surface lubricant film thickness near the exit. Therefore, simple discharge coefficient values for nozzle-diffuser cannot be used in this case, as the opposing ring is very close to the diffuser's exit, hence acting as a baffle. Idel'chik[16] provided tables and graphs, based on which the discharge coefficients for various configurations may be obtained. The closest case to the current configuration is the case of a rectangular edge diffuser opposing a baffle. However, the data does not cover the very low h_0/d ratios which are encountered in this case. Therefore, using extrapolation of the available data, a curve fit equation in the form of a third-order polynomial is made as follows:

$$K=-520\left(\frac{h_0}{d}\right)^3+418\left(\frac{h_0}{d}\right)^2-111.2\left(\frac{h_0}{d}\right)+10.53. \tag{4}$$

Rearranging the terms in the Bernoulli's equation, the supply pressure to the oil feedhole is obtained as follows:

$$p_s=\frac{\rho_s}{\rho_r}p_r+\frac{8}{\pi^2}\dot{m}^2\left[\frac{\rho_s}{\rho_r^2 d_0^4}+\frac{1}{\rho_s d^4}\left(16\pi\frac{\eta_s l}{\dot{m}}+K-1\right)\right]. \tag{5}$$

Lubricant rheological properties are evaluated, depending on the prevailing conditions. These are in terms of pressure and/or temperature upstream of the oil supply and recess conditions. The corresponding rheological relationships are given by Equations (11)–(14). As the prevailing conditions may not be known a priori, one would need to re-evaluate the lubricant density and viscosity at the calculated pressures.

The applied sealing load due to hydraulic cylinders, F, should be balanced by the hydrostatic generated contact pressures at the oil feedholes and in their vicinity. Considering that there are three such oil feedholes, the film thickness is obtained as follows:

$$h_0=\left\{\frac{9\eta_r\dot{m}}{F_c}\left[\left(\frac{r_o-r_i}{2}\right)^2-r_0^2\right]\right\}^{1/3}. \tag{6}$$

Using this evaluated seal gap, the mass flow rate and the required supply pressure at each oil feedhole can be calculated using Equations (1) and (5), respectively.

Neglecting viscous shear due to the dominance of pressure gradient (Poiseuille flow) in the contact, the friction torque is obtained as follows:

$$T_f=\frac{\pi}{4}\frac{\eta_r\omega}{h_0}(r_o+r_i)^2\left(r_o^2-r_i^2\right). \tag{7}$$

3.2 | Numerical analysis based on the Reynolds equation

Due to the presence of recessed features in the contact, it is expected that hydrodynamic pressures will be generated

in addition to the hydrostatic pressures predicted by the above-described analytical model. Therefore, a detailed numerical model is envisaged in addition to the aforementioned simplified analytical hydrostatic approach. Predictions from such a model can be compared with the purely hydrostatic analytical approach for generated friction, power loss and lubricant leakage. This approach ascertains the extent of hydrodynamic action and its necessity in promoting the necessary load carrying capacity for effective sealing. It is assumed that the seal operates under steady state conditions with laminar lubricant flow, and with the generated pressures not causing any local elastic deformation of the sealing rings. Any misalignment of sealing rings is also ignored. However, in practise misalignment, waviness, and thermal distortion of face seals can occur and lead to localised high pressures and thermal-elastohydrodynamic conditions.[1,17] Some representative misaligned analysis is provided by Haardt and Godet.[18]

Reynolds equation is commonly used for the analysis of mechanical face seals.[19] Considering the contact dimensions in the radial and circumferential directions and comparing these with the gap between the two seal rings, the necessary conditions for applying Reynolds assumptions are satisfied.[19] However, for mechanical face seals with thick lubricant films, significant lubricant inertial effects can exist as described by Dobrica and Fillon.[20] Therefore, a CFD approach is also undertaken later to re-examine the validity of the Reynolds-based model for the current analysis. Reynolds equation in cylindrical (polar) coordinates is expressed as follows[21]:

$$\frac{1}{r}\frac{\partial}{\partial r}\left(\frac{\rho h^3}{6\eta} r \frac{\partial p}{\partial r}\right) + \frac{1}{r^2}\frac{\partial}{\partial \theta}\left(\frac{\rho h^3}{6\eta}\frac{\partial p}{\partial \theta}\right) = \omega \frac{\partial(\rho h)}{\partial \theta} + 2\frac{\partial(\rho h)}{\partial t}. \tag{8}$$

The gap between the two opposing surfaces at any point can be written as a function of the minimum gap (or minimum film thickness), h_0, and the profile of the solid contacting surfaces, s as follows:

$$h(r, \theta, t) = h_0(t) + s(r, \theta). \tag{9}$$

The geometry of the recess is approximated by a half-ellipsoid. Therefore, the seal surface profile, incorporating the recesses as:

$$s(r, \theta) = \begin{cases} h_r \sqrt{1 - \left[\left(\frac{r - r_m}{b/2}\right)^2 + \left(\frac{(r + r_m)(\theta - \theta_n)}{a}\right)^2\right]} & \text{for } (r,\ \theta) \in A_r, \\ 0 & \text{for } (r,\ \theta) \notin A_r. \end{cases} \tag{10}$$

where, h_r is the maximum recess height, r_m is the mean radius at the radial location of the oil feed-holes, a and b are the semi-major and semi-minor axes of the elliptical recess cross-sectional profile, θ_n is the angular position of the n^{th} oil feed-hole and A_r is the area of the contact exposed to the recesses.

During the operation of the seal as the pressure and temperature rise, the lubricant density and viscosity alter. The variation of lubricant density with temperature and pressure is given as[22,23]:

$$\rho = \rho_0[1 - \gamma(T - T_0)]\left[1 + \frac{6 \times 10^{-10}(p - P_{atm})}{1 + 1.7 \times 10^{-9}(p - P_{atm})}\right], \tag{11}$$

where ρ_0 is the measured density at atmospheric pressure, P_{atm}, and ambient temperature, T_0 and γ is the coefficient of thermal expansion of the lubricant.

It is not expected that the generated pressures in the contact would be high enough to affect the lubricant viscosity significantly. Nevertheless, for the sake of completeness of the analysis, lubricant viscosity variation with pressure is considered through use of Roeland's expression[24]:

$$\eta = \eta_0 \exp\left\{\ln\left(\frac{\eta_0}{\eta_\infty}\right)\left[\left(1 + \frac{p - P_{atm}}{C_p}\right)^Z - 1\right]\right\}, \tag{12}$$

where η_0 is the lubricant dynamic viscosity measured at atmospheric pressure, P_{atm}, and ambient temperature, T_0, and parameters $\eta_\infty = 6.31 \times 10^{-5}$ Pa.s and $C_p = 1.98 \times 10^8$ Pa are constants.[14]

In addition, Z is the Roelands' pressure-viscosity index[25] and is independent of any variations in pressure:

$$Z = \frac{C_p \alpha}{\ln(\eta_0/\eta_\infty)}, \tag{13}$$

where α is the lubricant piezo-viscous coefficient.

To take into account variations of lubricant viscosity with temperature, Vogel's equation is used[14]:

$$\eta = \eta_c \exp\left(\frac{\beta}{T - T_\infty}\right). \tag{14}$$

The variation of lubricant viscosity with temperature was measured using a Hydra-motion resonant viscometer with the operational temperature range of −20°C to 120°C. In the equation above, the temperature at which the lubricant has infinite viscosity, T_∞, the inherent thermo-viscous coefficient of the lubricant, β, and the 'thickness' of the lubricant, η_c, are obtained as[26]:

$$T_\infty = \frac{\vartheta T_{mid} - \varrho T_{max}}{\vartheta - \varrho} \tag{15}$$

in which,

$$\vartheta = \ln\left(\frac{\eta_{T\min}}{\eta_{T\mathrm{mid}}}\right)/\ln\left(\frac{\eta_{T\min}}{\eta_{T\max}}\right),$$
$$\varrho = (T_{\mathrm{mid}} - T_{\min})/(T_{\max} - T_{\min}), \text{ and} \quad (16)$$
$$\beta = \frac{(T_{\min} + T_\infty)(T_{\mathrm{mid}} + T_\infty)}{(T_{\mathrm{mid}} - T_{\min})}\ln\left(\frac{\eta_{T\min}}{\eta_{T\mathrm{mid}}}\right),$$

$$\eta_c = \frac{1}{M}\sum_{m=1}^{M}\exp\left(\ln\eta_m - \frac{\beta}{T_m - T_\infty}\right), \quad (17)$$

where $T_{\min}$, $T_{\max}$ and T_{mid} are the minimum, maximum and middle temperatures for which the viscosity of the lubricant was measured. The parameters $\eta_{T\min}$ and $\eta_{T\mathrm{mid}}$ are the measured viscosities at the minimum and middle temperatures, and M is the total number of measurements.

Figure 3 shows the variation of dynamic viscosity with temperature for both the measured and curve-fitted data using Vogel's equation.[14]

For a simultaneous solution of the Reynolds equation, film thickness shape and the lubricant rheological state equations, boundary conditions for the computational domain should be defined. In the radial direction, the pressure at the inner and outer radii of the seal is atmospheric. This condition represents the in situ seal in the devised test rig. It should be noted that in real mixers, the exposed seal side to the mixing chamber experiences higher pressures than atmospheric. This can be easily accommodated by setting the pressure at the corresponding edge to the mixing chamber pressure. Therefore, in general form, the boundary conditions for pressure, in the radial direction, can be summarised as follows:

$$p(r_i, \theta) = P_i \quad \text{and} \quad p(r_o, \theta) = P_o. \quad (18)$$

Since the entire contact is modelled, in the circumferential direction, the following periodic condition for pressure is applied:

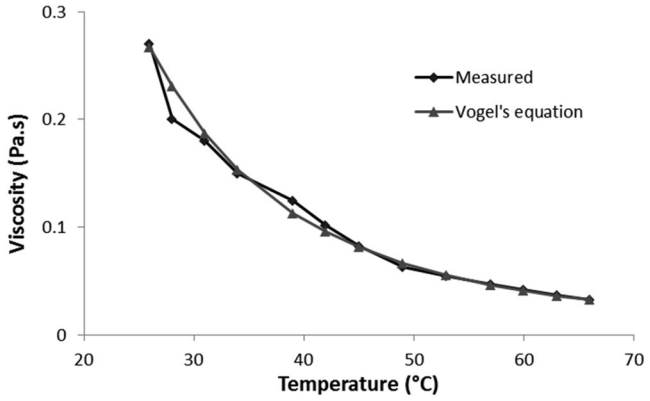

FIGURE 3 Measured and curve-fitted viscosity variation with temperature

$$p(r, 0) = p(r, 2\pi). \quad (19)$$

Any evaluated pressures below the atmospheric pressure indicate presence of cavitation. In order to take cavitation into account Swift[27] -Stieber[28] (or Reynolds exit boundary) condition are used in the analysis to determine the position of lubricant film rupture. Sliding occurs in the circumferential direction with no relative motion occurring in the radial direction. Thus, the boundary conditions become:

$$p(r, \theta_c) = P_c \quad \text{and} \quad \frac{\partial p}{\partial\theta}|_{(r,\,\theta_c)} = 0. \quad (20)$$

By setting the pressure at all computational mesh points equal to the cavitation vaporisation pressure of the lubricant in each iteration cycle, both conditions in Equation (20) are automatically satisfied.[29] For the current analysis, the cavitation pressure is assumed to be the same as the atmospheric pressure (i.e., $P_c = P_{\mathrm{atm}}$). Whenever pressures fall below the atmosphere, ambient air would immediately enter into the contact from the periphery of the seal exposed to the environment. Therefore, it is expected that gaseous cavitation would be presented.

The generated pressures in the lubricant entry recesses should be determined when solving Reynolds equation as: the flow rate at the oil feedholes is known, the generated pressure at the feedhole exit to the recess is obtained through an iterative procedure. Detailed calculations are provided below. The pressures at the oil feedholes determine the hydrostatically applied contact force.

To control the seal contact, the hydraulic and spring (closing) forces acting at the rear of the gland ring should balance the hydrostatic/hydrodynamic generated reaction (the opening forces). This equilibrium yields a gap filled with the lubricant guarding against undue friction and power loss, whilst minimising the lubricant quantity. In addition, wear of seal surfaces is mitigated, enhancing its durability. The observed significant leakage of lubricant in practise indicates that the operating gap is larger than one would expect of an effective seal. This is one of the motivations for the current study.

Table 1 lists the calculated applied contact load through hydraulic cylinders, based on the pressures produced by the hydraulic supply pump.

The pressure distribution obtained through solution of the Reynolds equation comprises both hydrostatic and hydrodynamic contributions. The total opening force becomes

$$F_o = \int\int prd\theta dr. \quad (21)$$

TABLE 1 Contact loads generated by the hydraulic cylinders

Pump pressure (bar)	Force per cylinder (N)	Total Force on seal faces (N)
10	804	2412
20	1608	4824
30	2412	7236
40	3216	9648
50	4020	12 060
60	4824	14 472

There are two main parameters which best describe the sealing performance. These are the power loss and lubricant leakage. The frictional power loss normally translates into generated heat, thus a rise in operating temperature, as well as potential thermo-elastic seal distortion. The power loss from the sealing contact is a function of the rotational speed and friction, which itself is a function of sliding speed.

Viscous friction comprises two components; one due to Poiseuille flow and the other because of sliding shear (i.e., Couette flow). The total friction due to viscous shear of the lubricant in contact becomes[13,21,26]:

$$f_v = \int\int |\overrightarrow{\tau_v}| r d\theta dr, \tag{22}$$

where viscous shear is

$$\overrightarrow{\tau_v} = \tau_{v,r}\hat{r} + \tau_{v,\theta}\hat{\theta} \tag{23}$$

in which

$$\tau_{v,r} = \pm\frac{h}{2}\frac{\partial p}{\partial r} \text{ and } \tau_{v,\theta} = \pm\frac{h}{2}\frac{\partial p}{r\partial\theta} + \frac{\eta r\omega}{h}, \tag{24}$$

where the negative sign is used for the moving surface. The coordinate system is attached to the stationary opposing surface (positive sign). The frictional power loss is obtained as follows:

$$P_l = \int\int |\overrightarrow{\tau_v}| \omega r^2 d\theta dr. \tag{25}$$

The frictional torque resisting the applied driving torque is

$$T_f = \int\int \tau_{v,\theta} r^2 d\theta dr. \tag{26}$$

The volumetric flow rate (leakage) is calculated by integrating the flow flux through the boundaries of the seal as follows:

$$\dot{Q}_l = \oiint \vec{v} d\vec{A}_s, \tag{27}$$

where A_s is the total side-leakage area around the edges of the seal gap and v is the velocity of the lubricant at these boundaries. Since the mass flow rate per unit circumferential length at both the inner and the outer radii is known, the leakage mass flow rate can be obtained as follows:

$$\dot{m}_l = \int_{\theta=0}^{2\pi} \dot{m}_r|_{r_i} r_i d\theta + \int_{\theta=0}^{2\pi} \dot{m}_r|_{r_o} r_o d\theta, \tag{28}$$

where the mass flow rate at any radial position is

$$\dot{m}_r = -\frac{\rho h^3}{12\eta}\frac{\partial p}{\partial r}. \tag{29}$$

If the integration of mass flow rate over either of the inner or the outer boundary radii becomes negative, then a leakage volume is obtained.

3.2.1 | Method of solution

Finite difference method (FDM) with Gauss–Seidel point successive over-relaxation (PSOR) iterations[30] is used to solve the Reynolds equation and obtain the generated pressure distribution:

$$p_{i,j}^k = (1-\varepsilon_p)p_{i,j}^{k-1} + \varepsilon_p p_{i,j}^k; \text{ where } \varepsilon_p \in (0, 2). \tag{30}$$

The value for over/under-relaxation factor is largely problem-dependent.[30] Through numerical testing an optimum value of $\varepsilon_p \simeq 1.0$ is obtained for the current analysis. The value of unity indicates that no under or over-relaxation is required in this case. The following convergence criterion for generated pressures is used. Therefore,

$$\mathrm{Er_p} = \frac{\sum_{i=1}^{I}\sum_{j=1}^{J}|p_{i,j}^k - p_{i,j}^{k-1}|}{\sum_{i=1}^{I}\sum_{j=1}^{J}p_{i,j}^k} \le \epsilon_p, \tag{31}$$

where in this case: $\epsilon_p = 1 \times 10^{-5}$.

The iterative procedure is summarised as follows:

1. Assume an initial minimum film thickness and determine the film shape.
2. For a given flow rate through the oil feedholes, assume an inlet pressure at the oil feed-holes.
3. Assume an initial contact pressure distribution.
4. Update the corresponding rheological parameters; lubricant density and viscosity for given pressures and at the measured operating temperature.
5. Apply the boundary conditions.
6. Compute pressure distribution through solution of discretised Reynolds, using the PSOR iterative method.
7. Integrate the hydrodynamic pressures over the contact area to obtain the generated opening force (lubricant reaction).
8. Calculate the oil leakage from the contact and compare it with the given inlet flow rate at the oil feedholes by applying the following convergence criterion:

$$\mathrm{Er}_F = \frac{|\dot{m}_{in} - \dot{m}_l|}{\dot{m}_{in}} \leq \epsilon_F, \tag{32}$$

where typically: $\epsilon_F \leq 1 \times 10^{-3}$.

If $\dot{m}_{in}$ is the inlet mass flow rate exceeds the above convergence criterion set for the flow balance between the inlet and outlet, then update the assumed inlet lubricant feed pressures at the oil feedholes as follows:

$$p_{in}^{\varphi+1} = \left(1 + \varepsilon_{\mathrm{F}} \frac{\dot{m}_{in} - \dot{m}_l}{\dot{m}_{in}}\right) p_{in}^{\varphi}, \tag{33}$$

where ε_{F} is the numerical damping coefficient (typically, $\varepsilon_{\mathrm{F}} \simeq 0.55$) for the flow iteration loop and φ is the current flow iteration loop.

9. Repeat the steps 3 to 8 using the newly calculated inlet lubricant fee pressure until the criterion for flow balance is satisfied.
10. Compare the calculated load carrying capacity of the contact (the opening force) with the applied contact load (the closing force), using the following load convergence criterion:

$$\mathrm{Er}_{\mathrm{L}} = \frac{|F_{\mathrm{c}} - F_o|}{F_{\mathrm{c}}} \leq \epsilon_F, \tag{34}$$

where the limit of convergence is typically, $\epsilon_{\mathrm{F}} \leq 1 \times 10^{-3}$.

If the equilibrium condition is not satisfied, then update the minimum oil film thickness as follows:

$$h_{\mathrm{m}}^{\phi+1} = \left(1 + \varepsilon_{\mathrm{L}} \frac{F_{\mathrm{o}} - F_{\mathrm{c}}}{F_{\mathrm{c}}}\right) h_{\mathrm{m}}^{\phi}, \tag{35}$$

where ε_L is a numerical damping coefficient (typically, $\varepsilon_L \simeq 0.055$) for the load balance iteration loop and ϕ is the current load loop.

11. Repeat Steps 2 to 10 using the newly calculated minimum film thickness until the criterion for load balance is satisfied.
12. Finally, calculate the performance parameters based on the calculated minimum film thickness, shape, and the corresponding pressure distribution.

For the current analysis, the computational mesh typically included 23×1187 finite differences in the radial and circumferential directions, respectively.

3.3 | Computational fluid dynamics (CFD) analysis approach

With formation of thick films and high flow rates, the effect of lubricant inertial flow and turbulence can become important. Furthermore, at the peripheral edges of the seal, exposed to the environment, promoting side leakage flow with reduced contact pressures, multi-phase flow as well as cavitation can occur. These issues are not accounted for in the Reynolds-based numerical analysis described above. Therefore, it is important to undertake detailed mass-conserving analysis, based upon the solution of Navier–Stokes equations in order to ascertain the validity of the less computationally rigorous analytical and numerical Reynolds solutions.

The CFD approach is based on similar analyses highlighted in more detail by Shahmohamadi et al[31,32] for the case of journal bearings and piston compression ring respectively. The governing equations for conservation of mass and momenta are:

$$\frac{D\rho}{Dt} + \rho \vec{\nabla}.\vec{v} = 0, \tag{36}$$

$$\rho \frac{D\vec{v}}{Dt} = -\vec{\nabla} p + \vec{\nabla}.\left[\eta\left(\frac{\partial U_i}{\partial x_j} + \frac{\partial U_j}{\partial x_i} - \frac{2}{3}\delta_{ij}\vec{\nabla}.\vec{v}\right)\right] + \vec{F}, \tag{37}$$

where D/Dt is the covariant (material) derivative operator, $\vec{\mathrm{F}}$ is the body force field vector, and δ_{ij} is the Kronecker delta.

3.3.1 | Boundary conditions and solution procedure

The system of Equations (36) and (37) is solved using the finite volume method (FVM). Figure 4 shows the computational domain with the associated boundary conditions. Hexahedral elements are used with the hexa-dominant meshing scheme. The entire flow domain is meshed using approximately 130 000 hexahedral computational cells.

Pressure staggering option was chosen for pressure interpolations with semi-implicit method for Pressure-Linked (SIMPLE) equations for pressure–velocity coupling.[33] This approach is used for tribological contacts by Shahmohanadi et al.ss,[31,32] and in conjunction with cavitation in rig-cylinder liner contact.[34] Momenta are solved using the second-order accurate scheme. As for the inlet boundary conditions, a constant flow rate of lubricant is applied. A pressure outlet boundary condition is implemented downstream, where the gradients of all the variables are set to zero in the normal orthogonal direction. No-slip boundary conditions are applied at all the solid boundaries.

4 | RESULTS AND DISCUSSION

4.1 | Effect of flow rate

Figure 5 shows the variation of seal gap and the generated frictional torque with the lubricant flow rate, using the simplified analytical method, as well as the Reynolds-based numerical analysis. It should be noted that the rise in the flow rate in each case is not linked to any previous case. Therefore, the results are for steady-state conditions for each stated flow rate, excluding the effect of transience. The lubricant film thickness (seal gap) increases with any rise in the lubricant flow rate, whilst the frictional torque reduces accordingly. As a result, it is expected that the generated contact heat would be reduced with a decreasing frictional power loss. In addition, any rise in the flow rate increases the convective heat transfer because of passage of lubricant through the contact. This would also result in a further reduction in temperature of the sealing surfaces. However, the downside would be the rise in the potential penetration of the powder/rubber compound from the chamber into the seal contact due in the presence of an increasing sealing gap at higher flow rates.

The numerical predictions show that a 6-fold rise in the flow rate would result in an approximately 50% reduction in viscous friction due to roughly a two-fold increase in the lubricant film thickness. It can also be observed that the analytical method predicts a lower film thickness compared with that of the numerical model. This difference can be better explained if the predicted injection pressures by both models are compared. Figure 6 shows the variations in injection pressure with the flow rate predicted by both the analytical and the numerical models.

The required injection pressure to maintain a given flow rate in each case, using the analytical model is twice that of the numerical method. There are two reasons for this difference. First, it relates to the assumptions made in determining the high-pressure area at the lubricant injection hole. Concentration of high pressures in smaller estimated areas used in the simplified analytical approach can account for this difference. Second, the analytical method is purely based on hydrostatic effect, which affects the contact load carrying capacity, thus a

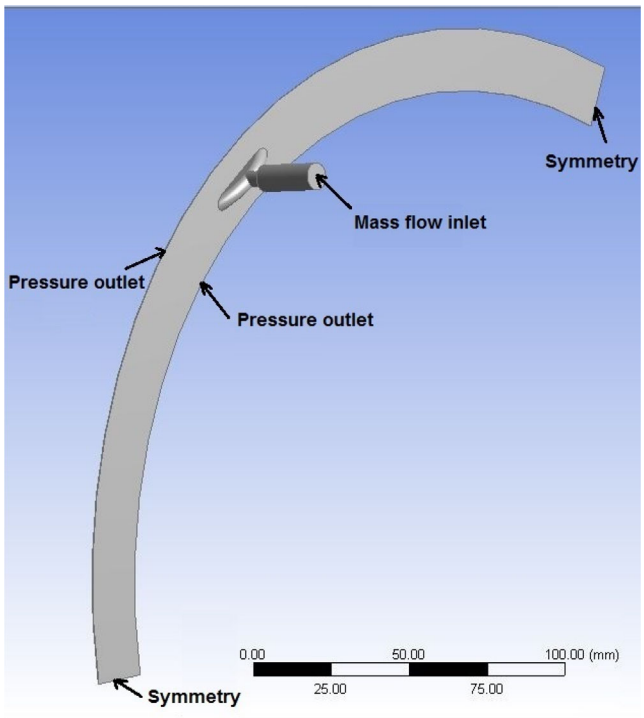

FIGURE 4 The computational domain and the applied boundary conditions

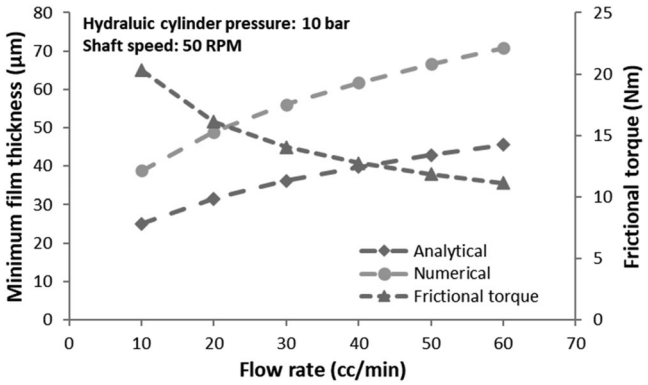

FIGURE 5 Effect of flow rate at the oil injection points upon seal performance

higher injection pressure would be required to sustain the same flow rate compared with the combined hydrostatic-hydrodynamic effect accounted for in the numerical analysis.

4.2 | Effect of hydraulic cylinder pressure

Figure 7 shows the effect of an increasing applied hydraulic cylinder pressure (i.e., the closing pressure) on the seal gap (minimum film thickness) and the generated frictional torque for a constant lubricant flow rate. As it would be expected, increasing the closing force results in a reduction in the sealing gap. Consequently, there is an increase in generated friction. Since the flow rate is kept constant, the heat rejection rate would remain unaltered. Therefore, a rise in contact temperature would be expected with increasing friction.

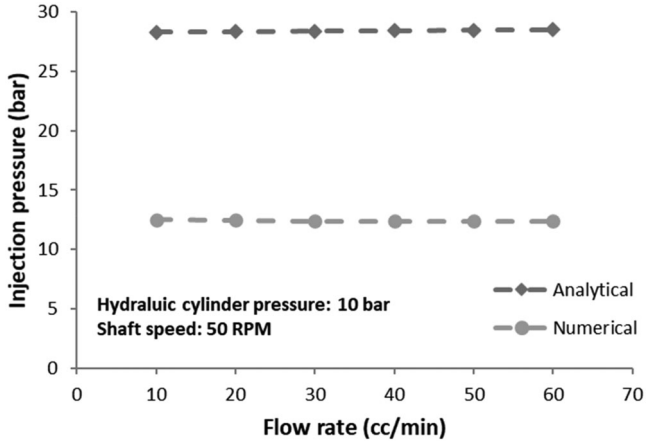

FIGURE 6 Predicted oil injection pressures at oil feedholes with different flow rates

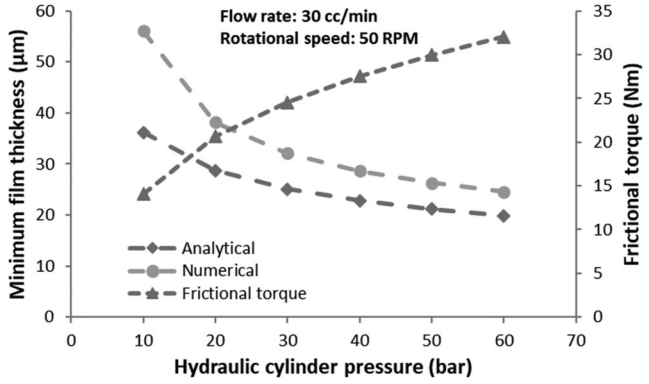

FIGURE 7 Effect of applied hydraulic pressure on the contact parameters

The analytical predictions show thinner film thickness compared with numerical predictions, again indicating under-estimation of contact load carrying capacity with the simplified hydrostatic analytical method.

An interesting observation in Figure 8 is the linear relationship found between the required injection pressure at the oil feed-holes and the applied hydraulic pressures. In the case of numerically predicted results, the slope of the line is approximately 2.5 for the given operating conditions.

4.3 | Comparison of the analytical and numerical results with CFD analysis

Comparisons are carried out for the predictions of the simplified analytical and Reynolds-based numerical models with those of the CFD model. Applying the similar iterative solution approach for load convergence as that noted above to a mass conserving CFD would require development of a moving mesh method, which due to the thinness of the lubricant film presents problems with the elemental aspect ratio, computational accuracy, and associated long computation times. For this reason, the film thickness values shown in Figure 5 are used in the CFD analysis to obtain the pressure distribution and load carrying capacity. Figure 9 shows the predicted load carrying capacity for all the developed models.

The results indicate that the predictions from the numerical and CFD results correlate quite well. The differences between the predictions of the three highlighted methods reduce with an increasing film thickness as the prevailing conditions tend to the dominance of hydrostatic effect (note that the analytical model is based on hydrostatics alone).

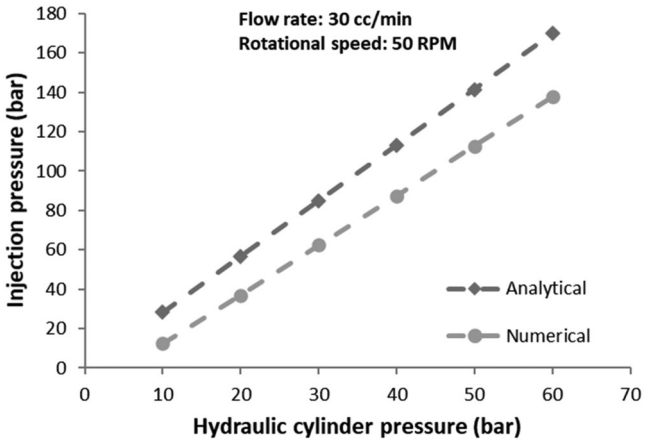

FIGURE 8 Predicted oil injection pressures at the oil feedholes with different closing pressures

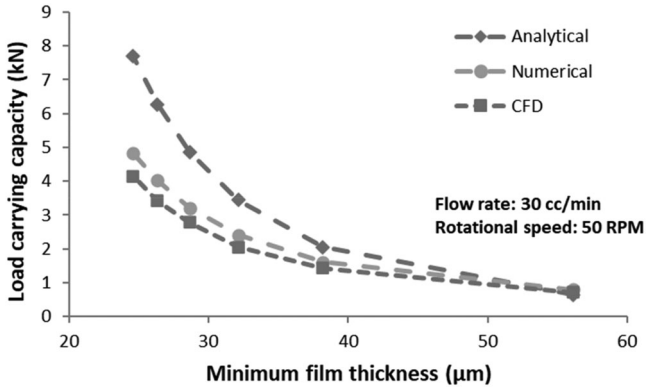

FIGURE 9 Load carrying capacity variation with film thickness

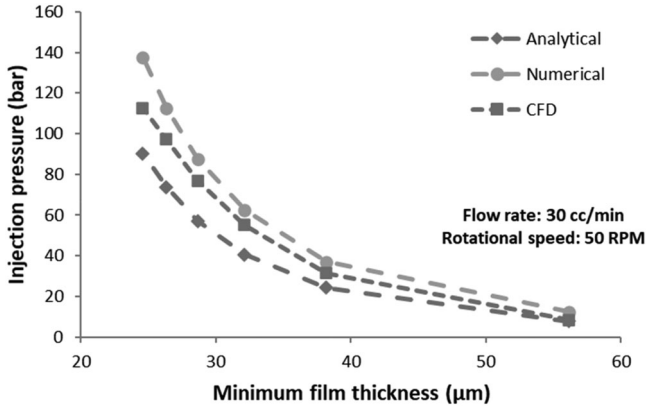

FIGURE 10 Predicted injection pressures

Figure 10 provides a comparison for the predicted injection pressures at the oil feedholes. Again, the results from the Reynolds-based numerical analysis are closer to the CFD analysis than those obtained through analytical approach, which under-estimates the injection pressures. This is another reason for the reduced load carrying capacity using the simplified analytical predictions. A conclusion reached is that the expounded analytical method provides good predictions for conditions pertaining to the dominance of hydrostatic load carrying capacity. This means that for ideally smooth (low waviness) and aligned seal faces with larger separations, the use of analytical method would suffice and is particularly advantageous in terms of its computational efficiency and timeliness within the industrial time-scales.

4.4 | Pressure distribution in the contact

Unlike the simplified analytical method, the Reynolds-based numerical analysis provides more detail, such as the generated contact pressure distribution over the sealing face. In practise this information helps the positioning of oil feed-holes in order to obtain a greater arc of lubricated contact around the seal periphery, mitigating friction and improving the load carrying capacity. Furthermore, this approach would enable the inclusion of surface waviness in detail as well as any contact misalignment. The same can be achieved with the CFD analysis,

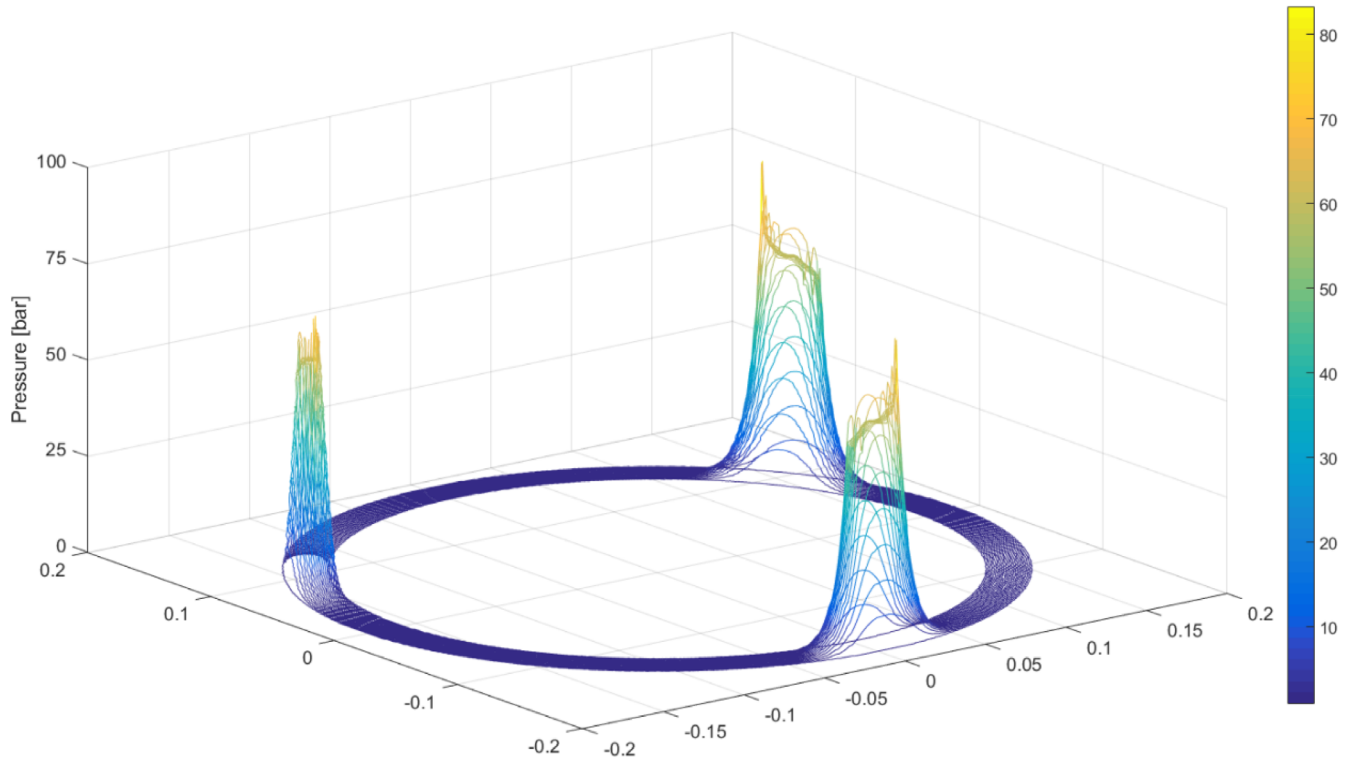

FIGURE 11 3D pressure distribution in the seal contact obtained through CFD

but with a greater degree of computational complexity and a significantly longer analysis time.

Figure 11 shows the pressure spikes in the vicinity of the oil feed-holes, reducing significantly away from these locations. Since the flow in the contact is in a counter-clockwise direction, the pressure spikes generated by the entrant lubricant are squeezed onto the opposing side of each recessed area. There is clearly a lack of any build-up of pressure in large areas of contact between successive recesses. An implication of this is loss of sealing and the potential ingression of abrasive mixture from the chamber into the seal contact, as well as poor retention of lubricant flow in the seal. The conclusion is that there is ineffective hydrodynamic effect for much of the seal contact. This is observed in practise by the inordinate leakage (thus use) of lubricant in most dust-stop seals.

5 | CONCLUDING REMARKS

Two methods, analytical and Reynolds-based numerical analysis are developed to study the performance of dust-stop seals of mixing chambers. The analytical model is based on the assumption of dominant hydrostatic action. Its predictions, whilst computationally time-efficient diverge from those of more complex numerical analysis, when combined hydrodynamic and hydrostatic conditions prevail in the seal contact caused by the seal's rotation. The validity of both developed methods is ascertained through application of computational fluid dynamics (CFD) analysis under quasi-steady conditions. This shows closer conformance of the numerical Reynolds-based predictions to the CFD analysis because of combined hydrostatic and hydrodynamic contact conditions as: well as more detailed pressure generation at the feed-holes for the entrant supplied lubricant.

The developed analytical-numerical model can be used to evaluate the performance of dust seals of mixing machines. The developed methods provide an explanation for an inordinate lubricant leakage from such machines. They also provide means of parametric study of dust-seals to improve upon their design and installation. The developed methodology will allow design and use of a scaled test-rig to further investigate the fundamental findings of the current research. Furthermore, the Reynolds-based numerical analysis tool may be further developed to include the effect of surface waviness of seal surfaces which occur during their manufacture and deemed to play a role in leakage as well as hydrodynamic flow. Combined with a dynamics analysis a more comprehensive approach may be developed to include the effect of seal misalignment which is also noted by uneven wear of surfaces in practise.

NOMENCLATURE

Roman symbols

A_r	recessed area
A_s	total peripheral gap area of the seal
a,b	semi-major and semi-minor axes of a recess elliptical cross-section
C_p	a rheological constant
d	diameter of an oil feed-hole
d_0	diameter of an equivalent circular recess
Er_F	calculated iterative error in lubricant flow
Er_L	calculated iterative error in contact load
Er_p	calculated iterative error of generated pressure
$\vec{F}$	body force field vector
F_c	closing force (applied contact load by hydraulic cylinders)
F_o	opening force
f_v	viscous friction
f_l	major loss coefficient
h	contacting profile
h_0	minimum film thickness
h_r	recess height
i,j	computational node
I,J	maximum number of mesh nodes in radial and peripheral directions
K	minor loss coefficient
l	length of the oil feed line
M	total number of viscosity measurements at various temperatures
m	measurement index
$\dot{m}$	mass flow rate
$\dot{m}_{in}$	inlet mass flow rate
$\dot{m}_l$	mass leakage flow rate
P_{atm}	atmospheric pressure
P_i,P_o	pressure at the inner and outer boundary radii
P_c	cavitation pressure
P_l	frictional power loss
p	absolute pressure
p_{in}	pressure at the inlet of a recess
p_r	pressure at the recess
p_s	static pressure at the upstream of an oil feed-hole
$\dot{Q}_l$	volumetric flow rate
Re	Reynolds' number
Re_d	Reynolds' number based on the oil feed-hole diameter
r	radius (radial coordinate)
r_0	radius of the equivalent circle
r_i,r_o	inner and outer radii of the seal contact
r_m	mean radius
r,θ,z	radial, circumferential and axial directions in cylindrical coordinates
$\hat{r},\hat{\theta},\hat{z}$	unit vectors in radial, circumferential and axial directions
s	seal profile in the circumferential direction

T temperature
T_0 ambient temperature
T_∞ theoretical asymptotic temperature for infinite lubricant viscosity
T_f frictional torque
t time
$\vec{v}$ velocity vector
v_r injection flow velocity at the recess exit
v_s injection flow velocity at the upstream of oil feed-hole
W_c load carrying capacity at each oil feed-hole area
Z Roelands' pressure-viscosity index

Greek symbols

α piezo-viscous parameter
β thermo-viscous coefficient
γ thermal expansion coefficient of the lubricant
δ_{ij} Kronecker delta
ε_F damping coefficient for inlet pressure update
ε_L damping coefficient for minimum film thickness update
ε_p (under/over-) relaxation factor for pressure calculations
ϵ_F convergence criterion for iterative flow calculations
ϵ_L convergence criterion for iterative load calculations
ϵ_p convergence criterion for iterative pressure calculations
η dynamic viscosity of lubricant
η_0 dynamic viscosity of lubricant at atmospheric pressure
η_r dynamic viscosity of lubricant at recess
s_s dynamic viscosity of lubricant at the oil feed-hole upstream
η_∞ rheological constant
η_c 'thickness' of the lubricant
θ angular (circumferential) coordinate
θ_c angular positions of the cavitation rupture points
θ_n angular position of the oil feed-hole
ϑ intermediate parameter in Vogel's equation
ρ lubricant density
ρ_0 lubricant density at ambient temperature and pressure
ρ_r lubricant density at recess
ρ_s lubricant density at upstream of oil feed hole
ϱ intermediate parameter in Vogel's equation
$\vec{\tau}_v$ viscous shear stress
ω angular speed

Subscripts

max maximum
mid middle
min minimum
r in the radial direction or conditions at the recess
s conditions at the upstream of oil feedhole
v viscous
θ in the circumferential direction

Superscripts

k pressure iteration step
φ flow iteration step
$\varnothing$ load iteration step

ACKNOWLEDGMENTS

The authors would like to acknowledge the funding provided to this project by Innovate-UK under a Knowledge Transfer Partnership (KTP) programme between Loughborough University and Farrel Ltd.

DATA AVAILABILITY STATEMENT

The data that support the findings of this study are available from the corresponding author upon reasonable request.

ORCID

Ramin Rahmani https://orcid.org/0000-0002-6084-8842

REFERENCES

1. Lebeck AO. *Principles and Design of Mechanical Face Seals*. John Wiley & Sons; 1991.
2. Lipschitz, A., Bi-directional, non-contact face seal, U.S. Patent 5,143,384, issued September 1, 1992.
3. Goldswain, I.M. and Hignett, M.D.W., Mechanical seal containing a sealing face with grooved regions which generate hydrodynamic lift between the sealing faces, U.S. Patent 5,496,047, issued March 5, 1996.
4. Su H, Rahmani R, Rahnejat H. Performance evaluation of bidirectional dry gas seals with special groove geometry. *Tribol Trans*. 2017;60(1):58-69. doi:10.1080/10402004.2016.1146380
5. Pascovici MD, Etsion I. A thermo-hydrodynamic analysis of a mechanical face seal. *Trans ASME, J Tribol*. 1992;114:639-645.
6. Brunetiere N, Tournerie B. Study of hydrostatic mechanical face seals operating in a turbulent rough flow regime. *Trans ASME, J Tribol*. 2009;131(3):32202.
7. Su H, Rahmani R, Rahnejat H. Thermohydrodynamics of bidirectional groove dry gas seals with slip flow. *Int J Thermal Sci*. 2016;110:270-284. doi:10.1016/j.ijthermalsci.2016.07.011
8. Limper, A., Dust stop systems for internal mixers – an innovative approach, KGK Kautschuk Gummi Kunststoffe 58, Jahrgang, 2005, 7/8/2005, pp. 366–370.
9. Key WE, Salant RF, Payvar P, Gopalakrishnan S, Vaghasia G. Analysis of a mechanical seal with deep hydropads. *Tribol Trans*. 1989;32(4):481-489.
10. Rahmani R, Shirvani A, Shirvani H. Optimization of partially textured parallel thrust bearings with square-shaped micro-dimples. *Tribol Trans*. 2007;50(3):401-406. doi:10.1080/10402000701429261
11. Rahmani R, Rahnejat H. Enhanced performance of optimised partially textured load bearing surfaces. *Tribol Int*. 2018;117:272-282. doi:10.1016/j.triboint.2017.09.011

12. Braun MJ, Dzodzo M. Effects of hydrostatic pocket shape on the flow pattern and pressure distribution. *Int J Rotat Machs*. 1995;1(3–4):225-235.
13. Shen F, Chen CL, Liu ZM. Effect of pocket geometry on the performance of a circular thrust pad hydrostatic bearing in machine tools. *Tribol Trans*. 2014;57(4):700-714.
14. Gohar R, Rahnejat H. *Fundamentals of Tribology*. Imperial College Press; 2008.
15. Shames IH. *Mechanics of Fluids*. 4th ed. McGraw Hill; 2002.
16. Idel'chik IE. *Handbook of Hydraulic Resistance: Coefficients of Local Resistance and of Friction*. U.S. Department of Commerce; 1966.
17. Tournerie B, Danos JC, Frêne J. Three-dimensional modeling of THD lubrication in face seals. *Trans ASME, J Tribol*. 2001; 123(1):196-204.
18. Haardt R, Godet M. Axial vibration of a misaligned radial face seal under a constant closure force. *Trans ASLE*. 1975;18(1): 55-61.
19. Dobrica MB, Fillon M. About the validity of Reynolds s and inertia effects in textured sliders of infinite width. *Proc IMechE, Part J: J Eng Tribol*. 2009;223(1):69-78.
20. Dobrica MB, Fillon M, Pascovici MD, Cicone T. Optimizing surface texture for hydrodynamic lubricated contacts using a mass-conserving numerical approach. *Proc IMechE, Part J: J Eng Tribol*. 2010;224(8):737-750.
21. Pinkus O, Sternlicht B. *Theory of Hydrodynamic Lubrication*. McGraw-Hill, Inc; 1961.
22. Dowson D, Higginson GR. *Elastohydrodynamic Lubrication: The Fundamentals of Roller Gear Lubrication*. Pergamon Press; 1966.
23. Yang P, Cui J, Jin ZM, Dowson D. Transient elastohydrodynamic analysis of elliptical contacts; part 2: thermal and Newtonian lubricant solution. *Proc IMechE, Part J: J Eng Tribol*. 2005;219:187-200.
24. Roelands CJA. *Correlation Aspects of Viscosity–Temperature–Pressure Relationship of Lubricating Oils*, PhD Thesis. Delft University of Technology; 1966.
25. Houpert L. New results of traction force calculations in elastohydrodynamic contacts. *Trans ASME, J Tribol*. 1985;107: 241-245.
26. Cameron A. *The Principles of Lubrication*. Longmans; 1966.
27. Swift HW. The stability of lubricating films in journal bearings. *Min Proc IMechE*. 1932;233:267-288.
28. Stieber W. *Das Schwimmlager: Hydrodynamische Theorie des Gleitlagers*. Verein Deutscher Ingenieure (VDI) GmbH; 1933.
29. Christopherson DG. A new mathematical method for the solution of film lubrication problems. *Proc IMechE*. 1941;146: 126-135.
30. Hoffmann KA, Chiang ST. *Computational Fluid Dynamics for Engineers*. Vol I. A Publication of Engineering Education System; 1993.
31. Shahmohamadi H, Rahmani R, Rahnejat H, Garner CP, Dowson D. Big end bearing losses with thermal cavitation flow under cylinder deactivation. *Tribol Lett*. 2015;57:2. doi:10.1007/s11249-014-0444-7
32. Shahmohamadi H, Rahmani R, Rahnejat H, Garner CP, King PD. Thermo-mixed hydrodynamics of piston compression ring conjunction. *Tribol Lett*. 2013;51(3):323-340. doi:10.1007/s11249-013-0163-5
33. Patankar SV, Spalding DB. A calculation procedure for heat, mass and momentum transfer in three-dimensional parabolic flows. *Int J Heat Mass Transfer*. 1972;15(10):1787-1806.
34. Shahmohamadi H, Rahmani R, Rahnejat H, King P, Garner C. Cavitating flow in engine piston ring-cylinder liner conjunction. *In ASME Int Mech Eng Cong Exposit*. 2013;56314.

How to cite this article: Fatourehchi E, Shahmohamadi H, Rahmani R, Rahnejat H, Johnson M, Wilson I. Tribology of dust-stop seals of mixing machines. *Lubrication Science*. 2022;1-14. doi:10.1002/ls.1632